JGR Oceans

RESEARCH ARTICLE
10.1029/2017JC013704

Special Section:
Forum for Arctic Modeling and Observational Synthesis (FAMOS) 2: Beaufort Gyre phenomenon

Tracing the Imprint of River Runoff Variability on Arctic Water Mass Transformation

Erwin Lambert[1,2,3], Aleksi Nummelin[1,2,4], Per Pemberton[5], and Mehmet Ilıcak[6,7]

[1]Geophysical Institute, University of Bergen, Bergen, Norway, [2]Bjerknes Centre for Climate Research, Bergen, Norway, [3]Institute for Marine and Atmospheric Research, Utrecht University, Utrecht, the Netherlands, [4]Department of Earth & Planetary Sciences, Johns Hopkins University, Baltimore, MD, USA, [5]Swedish Meteorological and Hydrological Institute, Gothenburg, Sweden, [6]Eurasia Institute of Earth Sciences, Istanbul Technical University, Istanbul, Turkey, [7]NORCE Norwegian Research Centre, Bjerknes Centre for Climate Research, Bergen, Norway

Abstract The Arctic Ocean receives a net freshwater input from land and from the atmosphere. This flux of freshwater, along with net surface heat loss, acts to transform the water mass properties of inflowing Atlantic and Pacific waters. In this study, model simulations are used to quantify the Arctic water mass transformation in salinity and temperature space, and its explained variance due to variability in the largest freshwater source to the Arctic: river runoff. This explained variance is quantified using a novel tool, the seasonal climate response function, which describes the magnitude and time scale of adjustment to a runoff perturbation at monthly resolution. Using this method, the transient response of Arctic water mass transformation is reconstructed over time scales ranging from several months to a decade. Model simulations with variable runoff indicate a significant explained model variance of several terms contributing to salinity transformation, including diffusion, the formation and melt of sea ice, and a possibly model-dependent surface salinity-restoring term. Most notably, an increase in river runoff strengthens the diffusion of salt and heat, which ultimately leads to an increase in the advective salt and heat import into the Arctic. These results provide evidence for the potential predictability of the Arctic system based on variability in river runoff.

Plain Language Summary The outflow of rivers into the Arctic Ocean varies greatly from year to year and has a large impact on the waters, which are exchanged between the Arctic and the surrounding oceans. In this study, we use a numerical model to understand how variability in river outflow affects processes in the Arctic, such as the formation and melt of sea ice, and on what time scales. To describe the impact of river outflow on time scales from months to a decade, we present a simple mathematical tool that is compared to simulations from the numerical model. We find that this tool can be used to explain, and possibly predict, variations in Arctic processes based on knowledge of variations in river outflow. Interestingly, we find that an increase in river outflow increases the transport of heat to the Arctic and reduces the sea ice extent.

Key Points:
- Seasonal climate response function reveals potential predictability of regional climate processes at monthly resolution
- Runoff variability impacts Arctic water mass transformation on time scales from several months up to 10 years
- Increased Arctic runoff enhances heat import into the Arctic and surface heat loss

Correspondence to:
E. Lambert,
E.Lambert@uu.nl

Citation:
Lambert, E., Nummelin, A., Pemberton, P., & Ilıcak, M. (2019). Tracing the imprint of river runoff variability on Arctic water mass transformation. *Journal of Geophysical Research: Oceans*, *124*, 302–319. https://doi.org/10.1029/2017JC013704

Received 13 DEC 2017
Accepted 18 DEC 2018
Accepted article online 21 DEC 2018
Published online 14 JAN 2019

1. Introduction

The Arctic Ocean is a semienclosed basin, surrounded by vast continents and relatively narrow straits (Figure 1a). The Arctic is characterized by a significant modification of circulating water masses due to freshwater input and by cooling due to surface heat loss (Carmack et al., 2016; Rudels et al., 2015). This water mass transformation maintains a steady state circulation of inflowing warm, saline water, and two branches of outflow: one carrying cold fresh water and the other carrying cold dense water (Eldevik & Nilsen, 2013; Lambert et al., 2016; Rudels, 2010; Stigebrandt, 1985). Besides this steady state circulation, the Arctic exhibits a strong seasonality due to solar irradiance, the formation and melt of sea ice, and river runoff. In addition, the freshwater input by river runoff shows a considerable interannual variability (Haine et al., 2015). In this study, we use a numerical model to describe the transient impact of variable river runoff on water mass transformation in the highly seasonal environment of the Arctic.

Arctic river runoff affects water mass transformation both directly (through freshening of surface waters) and indirectly (e.g., through changes in stratification). In the long term, an increase in river runoff has been shown to increase the stratification and subhalocline temperatures in the Arctic (Nummelin et al.,

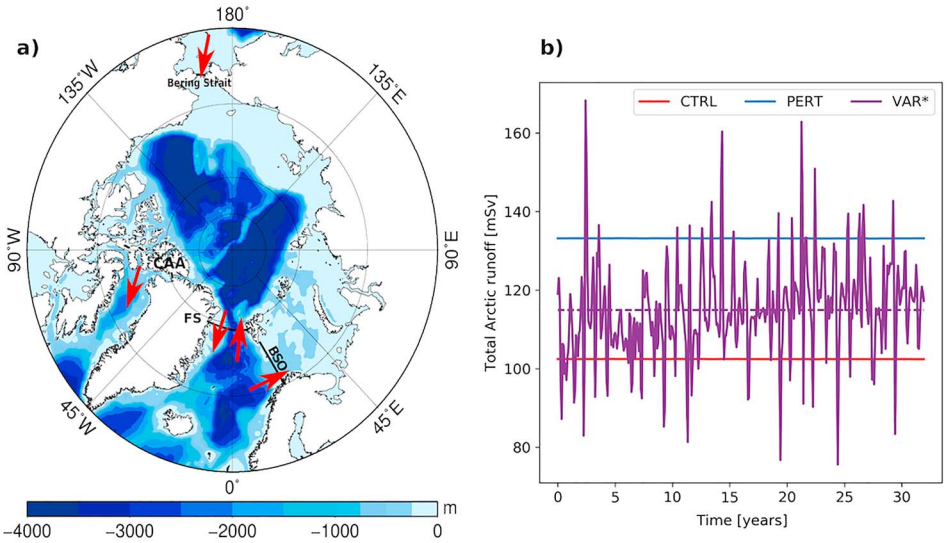

Figure 1. Arctic domain and river runoff. (a) Arctic Ocean with dominant inflows and outflows (red arrows). Blue shading indicates bathymetry. Surrounding gateways are Fram Strait (FS), Barents Sea Opening (BSO), Canadian Arctic Archipelago (CAA), and Bering Strait. (b) Total Arctic runoff for the three model experiments after spinup of 400 years. Runoff in the CTRL case is equal to that during spinup. Runoff in the PERT case is increased by 30% within the Arctic. Runoff in the VAR case is from the CORE-II data set. *For the VAR case, only the deseasonalized (solid) and mean (dashed) runoff is shown.

2015, 2016; Pemberton & Nilsson, 2016). A moderate increase in river runoff (<30%) can strengthen the exchanges of volume and heat with the surrounding oceans, whereas a larger increase can weaken these exchanges (Nummelin et al., 2016). Furthermore, Jahn, Tremblay, Mysak, et al. (2010) found an increase in the northward ocean heat transport with increased Arctic freshwater export. The impact of long-term changes in Arctic freshwater input may have consequences beyond the Arctic domain, as Lambert et al. (2016) suggested that increased Arctic runoff can stabilize the northern branch of the Atlantic thermohaline circulation. Although knowledge of these long-term impacts is important in light of the projected increase in Arctic river runoff, little is known of the short-term impacts of runoff variability.

The impact of variability in a forcing term, such as runoff, on climate processes has been studied using climate response functions (CRFs; Johnson et al., 2018; Kostov et al., 2017, 2018; Marshall et al., 2017). A CRF describes the magnitude and time scale of the response of a process to a change in forcing and can be estimated from a stepwise perturbation experiment (this study; Marshall et al., 2017) or from internal variability (Johnson et al., 2018; Kostov et al., 2017, 2018). Through convolution of this CRF with the forcing history, the variability in a climate process can be reconstructed. The benefit of this method with respect to other mathematical tools, such as lagged correlations, is that the CRF exploits the memory in the climate system. In general, the memory in a system arises from a finite system response time scale (e.g., Hasselmann et al., 1993; Van Hateren, 2013), which in our case is linked to the considerable residence time of river runoff in the upper Arctic Ocean ($\mathcal{O}$(10 years), Bauch et al., 1995; Jahn, Tremblay, Newton, et al., 2010; Pemberton et al., 2014). Consequently, one may expect that the variability in river runoff impacts Arctic water mass transformation for several years.

Arctic water mass transformation is characterized by the exchange of water masses with the surrounding basins and by surface and subsurface water mass transformation. This water mass transformation results in the modification of water masses derived from the North Atlantic and the North Pacific. Warm and saline Atlantic Water enters through the Barents Sea Opening and Fram Strait and relatively fresh and seasonally warm Pacific Water enters through Bering Strait (Rudels, 2015). In addition to this long-term mean circulation, eddies contribute to the net exchange of salt, heat, and mass across the Arctic gateways (von Appen et al., 2016; Hattermann et al., 2016). The surface fluxes of heat, salt, and freshwater are characterized by a strong seasonality. During winter, surface heat loss and brine rejection induce a net buoyancy loss of surface waters, whereas during summer, shortwave radiation, river runoff, and sea ice melt induce a net buoyancy gain. Integrated over a year, these surface fluxes prescribe a net cooling and freshening of inflowing

water masses as they circulate the Arctic Ocean. The outflows of these modified water masses exit primarily through Fram Strait and the Canadian Arctic Archipelago.

In this study we consider river runoff as an external forcing parameter, but we note that variability in runoff and other processes in the Arctic are linked to atmospheric variability. Through their manifestation in surface wind and pressure patterns, modes of extratropical Northern Hemisphere atmospheric circulation, such as the Arctic Oscillation (AO) and the North Atlantic Oscillation (NAO), affect the Arctic sea ice export (Guemas et al., 2016; Krahmann & Visbeck, 2003; Rigor et al., 2002; Smedsrud et al., 2011), freshwater export and its distribution within the Arctic (Anderson et al., 2004; Jahn, Tremblay, Mysak, et al., 2010; Johnson et al., 2018), and the northward heat transport in the Atlantic sector (Delworth & Zeng, 2016)—which further controls the mean winter sea ice edge (Bitz et al., 2002) and its variability (Årthun et al., 2012; Onarheim et al., 2015). The precipitation and snow cover in the Arctic region (Niederdrenk et al., 2016), and consequently the river runoff itself (Déry & Wood, 2004; Niederdrenk et al., 2016; Peterson et al., 2002), are linked to moisture pathways associated with the AO, the NAO, and the Pacific Decadal Oscillation on interannual to decadal time scales. The impact of variable river runoff thus ultimately describes a fraction of the atmospheric forcing of Arctic water mass transformation.

Both globally and in the Arctic, surface fluxes of heat and freshwater act to create the water mass extremes (Hieronymus et al., 2014; Pemberton et al., 2015), while diffusion and (locally) advection act to balance the effects of surface fluxes in steady state. This balance between surface fluxes, advection, and diffusion is described by the water mass transformation framework of Walin (1977, 1982), which we will use to diagnose Arctic water mass transformation. This framework describes salinity and temperature transformation in terms of salinity and temperature, respectively. This framework has been extended to study density transformation (Badin & Williams, 2010; Badin et al., 2013; Marshall, 1997; Marshall et al., 1999; Nurser et al., 1999; Sloyan & Rintoul, 2000, 2001; Speer & Tziperman, 1992; Tziperman, 1986), as well as the combination of salinity and temperature transformation in an S,T framework (Grist et al., 2016; Hieronymus et al., 2014; Pemberton et al., 2015; Speer, 1993). This S,T framework has formed the basis of transformation vectors describing water mass transformation in semienclosed basins (Pemberton et al., 2015; Speer, 1993) and stream functions in S-T space for transformation in the global ocean (Döös et al., 2012; Groeskamp, Zika, McDougall, et al., 2014; Hieronymus et al., 2014; Zika et al., 2012). More recently, Groeskamp et al. (2017) used the S,T framework to estimate ocean mixing from observations. All these applications are based on the steady state balance between advection, diffusion, and surface fluxes. In this study, we combine the framework with CRFs to study the temporal variability in water mass transformation.

In section 2 we formulate the CRFs, describe the water mass transformation framework, and present the numerical model setup. In section 3, we diagnose the control water mass transformation and extract the dominant processes that describe the Arctic system. In section 4, we compute CRFs for these processes and reconstruct the transient impact of river runoff variability. We end the paper with a discussion in section 5 and conclusions in section 6.

2. Methods

2.1. Seasonal CRF

In order to trace the imprint of variable river runoff on Arctic water mass transformation, we compute CRFs (e.g., Marshall et al., 2017). CRFs are response functions of some climate diagnostic D to an idealized perturbation in a forcing parameter R. Through convolution, a time series of D can be constructed from a time series of R. Here we will construct CRFs based on a step function increase in the total Arctic river runoff of 30%. We consider an idealized CRF by assuming that the response of any climate diagnostic D can be described in terms of an exponential decay toward a new equilibrium:

$$D(t) = \bar{D} + \delta(1 - e^{-t/\tau}). \tag{1}$$

Here t is the time after the perturbation; $\bar{D}$ is the control value of D. The CRF is determined by two parameters: The equilibrium sensitivity δ denotes the change in D after adjustment to the 30% increase in runoff, and the time scale τ is the associated e-folding time scale. Note that more general forms of CRFs have been presented (Johnson et al., 2018; Kostov et al., 2017; Marshall et al., 2017). By assuming that the response of D to variability in R is linear, one can construct a time series of D:

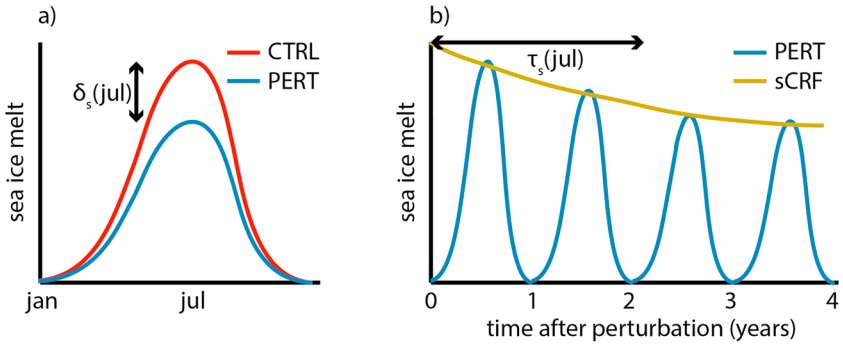

Figure 2. Visualization of the seasonal climate response function. (a) Steady state seasonal cycle for the idealized example diagnostic of sea ice melt. CTRL denotes the control values $\bar{D}_s(m)$; PERT denotes the values after equilibration to a perturbation $\bar{D}_s(m) - \delta_s(m)$. (b) The transient response to the perturbation; the adjustment time scale $\tau_s(m)$ is derived from the exponential fit denoted by sCRF. This process is repeated for each calendar month to determine the sCRF parameters δ_s and τ_s. sCRF = seasonal climate response function.

$$D(t) = \bar{D} + \frac{\delta}{\tau R_{\text{step}}} \int_{-\infty}^{t} R'(t') e^{-(t-t')/\tau} \mathrm{d}t'. \tag{2}$$

Here R_{step} is the magnitude of the step function increase in R used to compute δ, and R' is the anomaly in river runoff from the control value. Note that the assumption of linearity implies that δ and τ are independent of the magnitude of R'. The integral indicates that the value of D at each time t is the function of all values of R' before time t.

A CRF can provide useful information about the impact of the variability in runoff on diagnostic D if it adheres to a number of requirements. First, the impact of the variability in total Arctic river runoff R must be sufficiently large compared to other impacts of river runoff such as spatiotemporal variability. Second, the sensitivity δ must be sufficiently large with respect to the internal variability in $\bar{D}$; in other words, the signal-to-noise ratio must be sufficient. And third, the exponential function in equation (1) must adequately describe the adjustment to the step function increase in runoff.

We will assume that the spatiotemporal variability in Arctic river runoff is sufficiently small to be neglected. However, the other two requirements depend on the seasonality of diagnostic D. To illustrate this, we consider the example of total Arctic sea ice melt as climate diagnostic D. Sea ice melt in the Arctic dominates throughout the summer and is negligible during winter as schematically illustrated in Figure 2a. Although one can consider perturbations with respect to this mean seasonal cycle, the sensitivity δ will also vary throughout the season. Summer sea ice melt may be affected by increased river runoff, here depicted for illustration by a decrease, whereas winter ice melt will remain negligible irrespective of the amount of river runoff.

Because of the strong seasonal cycle in Arctic water mass transformation, we may expect the sensitivity δ of many climate diagnostics to contain a seasonal pattern. Furthermore, it is possible that the time scale τ varies throughout the season as well. This issue of seasonality is commonly surpassed by considering annual mean values of D and δ (e.g., Marshall et al., 2017). However, that approach limits the temporal resolution of the constructed time series to annual values as well. As we expect the impact of river runoff on Arctic water mass transformation to be considerable within years, we wish to retain a monthly resolution. For this, we introduce the seasonal CRF (sCRF).

The sCRF expands the common CRF by introducing seasonally dependent sensitivities and time scales. Whereas the common CRF is described by two parameters δ and τ, the sCRF is described by 24 parameters $\delta_s(m)$ and $\tau_s(m)$ where m is the calendar month. This seasonal dependency of the CRF parameters is illustrated in Figure 2 by contrasting the potential impact of a perturbation on sea ice melt in January and July. The complete sCRF is derived by computing $\delta_s(m)$ and $\tau_s(m)$ for each calendar month. From these values and a time series of forcing parameter R, the monthly time series of diagnostic D can be determined using

$$D(m) = \bar{D}_s(m) + \frac{\delta_s(m)}{\tau_s(m) R_{\text{step}}} \sum_{m'=-\infty}^{m-1} R'(m') e^{-(m-m')/\tau_s(m)}, \tag{3}$$

which is the seasonal equivalent of equation (2). Here the time series of both D and R are discretized into monthly averages by replacing time t with month m. The subscript s denotes seasonally dependent parameters, which depend on the calendar month corresponding to m. Note that this formulation of the sCRF only considers seasonality in the response to forcing variability and not in the forcing itself as done by Kostov et al. (2018). Equation (3) could be enhanced with a seasonal forcing by repeating the computation of the sCRF parameters for perturbations in different calendar months.

The computation of sCRF parameters δ_s and τ_s and the construction of $D(m)$ are performed off-line from monthly average model output. When the adjustment of some diagnostic D occurs within a month ($\tau_s < 1$ month), equation (3) cannot be applied. In this case, $D(m)$ is computed using a direct correlation between D and forcing parameter R, which is weighted by δ_s. In this case, memory in the system vanishes.

2.2. Water Mass Transformation

The diagnostics used to computed CRFs are extracted from the salinity and temperature frameworks of Walin (1977, 1982). This framework is based on the conservation of volume, salt, and heat within a certain range of salinities or temperatures. Within this framework, water mass transformation is interpreted as a volume flux across isohalines or isotherms as illustrated in Figure 3. Both the salinity and temperature frameworks describe a balance between three terms: net advection of volume out of the Arctic (M), diffusion of salt or heat (F^S, F^T), and surface fluxes of (virtual) salt or heat (SE, Q). Each salinity transformation term modifies the total volume of Arctic water with a salinity below S, denoted as $V(S)$, and each temperature transformation term modifies $V(T)$, the total volume of Arctic water with a temperature below T.

In steady state, the salinity framework describes the conservation of salt and volume within $V(S)$. The conservation of salt is expressed as

$$\int_{S_{\min}}^{S} M(S')\mathrm{d}S' = F^S(S) - SE(S) \tag{4}$$

and is illustrated in Figure 3c. Here $M(S)$ is the volume flux of water with a salinity below S, which is advected out of the Arctic across its surrounding gateways in cubic meters per second; $F^S(S)$ is the diffusive salt flux across isohaline S in grams per kilogram times cubic meters per second; and $SE(S)$ is the net (virtual) salt flux across all outcropping waters with a salinity below S in grams per kilogram times cubic meters per second. The advection includes both the long-term mean flow across the gateways as well as the short-term (eddy induced) variability; diffusion across these gateways is neglected in the budget. The surface salt flux includes both actual salt fluxes such as brine rejection, as well as freshwater fluxes such as river runoff; these freshwater fluxes are converted into virtual salt fluxes (e.g., Huang, 1993). The penetration of brine fluxes below the sea surface is included in the surface salt flux, though it transforms deeper and typically more saline layers (see Pemberton et al., 2015). The salinity framework is completed by conservation of volume within $V(S)$, which is expressed by the derivative of equation (4) with respect to salinity S,

$$M(S) = \frac{\partial F^S(S)}{\partial S} - \frac{\partial SE(S)}{\partial S} \tag{5}$$

and is illustrated in Figure 3e.

The temperature framework similarly describes the conservation of heat and volume within $V(T)$. Conservation of heat is expressed as

$$c\int_{T_{\min}}^{T} M(T')dT' = F^T(T) + Q(T) \tag{6}$$

and is illustrated in Figure 3d. Here c is the volumetric heat capacity in Joules per cubic meter per degree Celsius; $M(T)$ is the advection of water with a temperature below T across the Arctic gateways; $F^T(T)$ is the heat diffusion across isotherm T in watts; $Q(T)$ is the net surface heat flux across outcropping waters with a temperature below T in watts. As river runoff is treated as a virtual salt flux, it does not affect the heat budget. Similar to brine penetration, the penetration of solar heating below the sea surface is included in the surface flux, though it acts to transform deeper layers (e.g., Groeskamp & Iudicone, 2018; Iudicone et al., 2008). Finally, conservation of volume within $V(T)$ is expressed by the derivative of equation (6),

$$M(T) = \frac{1}{c}\frac{\partial F^T(T)}{\partial T} + \frac{1}{c}\frac{\partial Q(T)}{\partial T} \tag{7}$$

and is illustrated in Figure 3f.

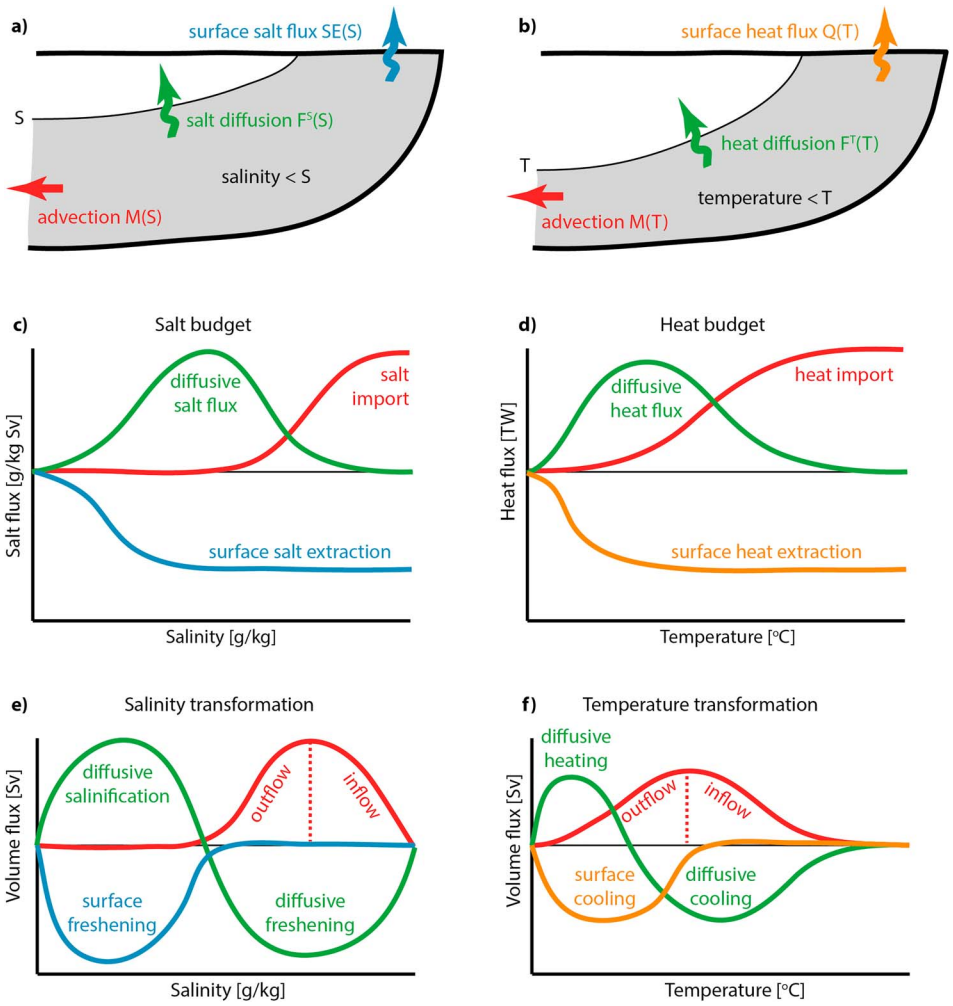

Figure 3. Visualization of Arctic water mass transformation in (a, c, e) the salinity framework and (b, d, f) the temperature framework. (a, b) The three balancing terms governing the salinity and temperature frameworks. (c, d) The cumulative salt and heat budgets corresponding to equations (4) and (6). (e, f) The salinity and temperature transformation corresponding to equations (5) and (7). Panels (a) and (b) are adapted from Pemberton et al. (2015). Note that isohaline S and isotherm T are purely for illustrative purposes and do not imply actual stratification.

Throughout the remainder of this paper, we will use the terms in equations (4)–(7) to describe water mass transformation in the Arctic. The transformation rates (equation (5) and (7)) are volume fluxes, which henceforth will be expressed in sverdrups (1 Sv $\equiv 10^6$ m^3/s). Note that these equations describe steady state balances and therefore do not hold at each moment in time. In order to resolve the transient state of the system, one could explicitly solve for the residual of these balances. However, we are particularly interested in the transient response of the water mass transformation terms themselves. To express this response, we will compute CRFs for the individual terms that describe the steady state balance.

2.3. Model Setup

We diagnose the salinity and temperature frameworks and compute sCRFs from model simulations using the coupled sea ice-ocean component of the Norwegian Earth System Model (Bentsen et al., 2013). The ocean model originates from the Miami Isopycnic Coordinate Model (MICOM, Bleck & Smith, 1990), but is extensively updated, and the sea ice component is the Los Alamos Sea Ice Model version 4 (Hunke et al., 2010). The sea ice and ocean components are fully coupled and configured on the same tripolar grid. The horizontal grid cells are optimized for isotropic grid spacing except toward the equator where the meridional resolution approaches 0.25° and is 1° zonal. The Northern Hemisphere grid singularities are located in Canada and Siberia. This gives a typical resolution in the Arctic ocean of approximately 40 km. The vertical grid consists of 51 isopycnic layers referenced to 2,000 dbar, with the surface mixed layer divided into two

nonisopycnic layers. The model includes a Gent-McWilliams parametrization as detailed in Danabasoglu et al. (2016). Further information of this version of the model setup can be found in Ilıcak et al. (2016).

The model is forced with Normal Year Forcing from the Coordinated ocean-ice experiments data set (CORE, Large & Yeager, 2004), which is an annually repeated cycle of atmospheric fluxes. This forcing suppresses other sources of interannual variability than runoff. The model forcing includes a sea surface salinity restoring to climatology, which is applied globally with a time scale of 6 days. As discussed by Ilıcak et al. (2016), the model has a prominent cold bias in the deep Arctic basin, though this was found not to significantly impact the heat transport into the Arctic. In addition, the model is known to have a cold and fresh bias in the mixed layer.

The model is spun up over 400 years, applying a constant runoff without a seasonal cycle. After this spinup, three simulations are performed over a period of 32 years with different river runoff fields into the Arctic Ocean (see Figure 1b). The CTRL case has the same runoff as during spinup; the PERT case has a stepwise runoff increase of 30% within the Arctic basin; and the VAR case has monthly runoff into the Arctic based on the Coordinated ocean-ice experiments-II data set (CORE-II, Large & Yeager, 2009). The latter contains a seasonal cycle, interannual variability, and spatiotemporal variability with a possible anticorrelation between the different river outlets. In all cases, runoff outside the Arctic is constant and unperturbed from the spinup and CTRL case.

To compute CRFs, we choose a 30% runoff perturbation as R_{step}, which is on the order of typical interannual variability (Figure 1b). This perturbation is small compared to simulations proposed by Marshall et al. (2017). By using simulations with Normal Year Forcing, external sources of interannual variability are suppressed. As a result, relatively small perturbations can exceed the stochastic variability, allowing for the computation of CRFs without the need for an ensemble of simulations. Such small perturbations are beneficial as they limit the probability of a nonlinear response that violates the theory of CRFs.

The steady state balances derived from the CTRL and PERT cases are based on averages from years 410 to 432. This allows for the system to adjust for one typical renewal cycle of Arctic freshwater, which is of $\mathcal{O}$(10 years), and allows for a relatively long time (22 years) to approximate statistical steady state. The diagnostics of all terms that compose the salinity and temperature frameworks are computed online in salinity bins of 0.04 g/kg and temperature bins of 0.04 ° C (equal resolution to Hieronymus et al., 2014; Pemberton et al., 2015). Note that we neglect any water mass transformation within each salinity and temperature bins and do not include a local response term as introduced by Groeskamp, Zika, Sloyan, et al. (2014). This resolution is relatively high compared to the isopycnal resolution of the model. As a consequence, the diagnostic output is strongly concentrated in a limited number of salinity and temperature bins, making the output strongly dependent on the specific model discretization. In order to derive physically realistic transformation fields, we apply an off-line smoothing in salinity of 0.8 g/kg and in temperature of 0.4 ° C to derive a relatively continuous diagnostic output.

3. Arctic Water Mass Transformation

In order to understand the impact of runoff variability on the water mass transformation in the Arctic Ocean, we first need to understand the control state. In this section, we discuss the long-term mean water mass transformation in terms of volume, salt, and heat budgets as described by equations (4)–(7). These budgets are diagnosed from the CTRL simulation, after reaching steady state, in terms of either salinity or temperature. From these balances, we extract several dominant balances that describe the basin-wide water mass transformation processes in the modeled Arctic Ocean. These balances form the background to which perturbations induced by runoff variability are analyzed in section 4.

3.1. Control Simulation

As schematically illustrated in Figure 3, water mass transformation can be described in terms of advection, diffusion, and surface fluxes of salt and heat. The salt, heat, and volume fluxes from the model simulation are shown in Figure 4.

The Arctic-wide salt budget is marked by the integrated salt fluxes below S_{max} (Figure 4a). As diffusion cannot act as a net source or sink of salt but can only redistribute salt within the basin, the total salt budget is governed by a balance between advection and surface salt fluxes. The negative surface salt flux reflects a net integrated surface freshwater input into the Arctic, and the positive advective salt flux across reflects a net

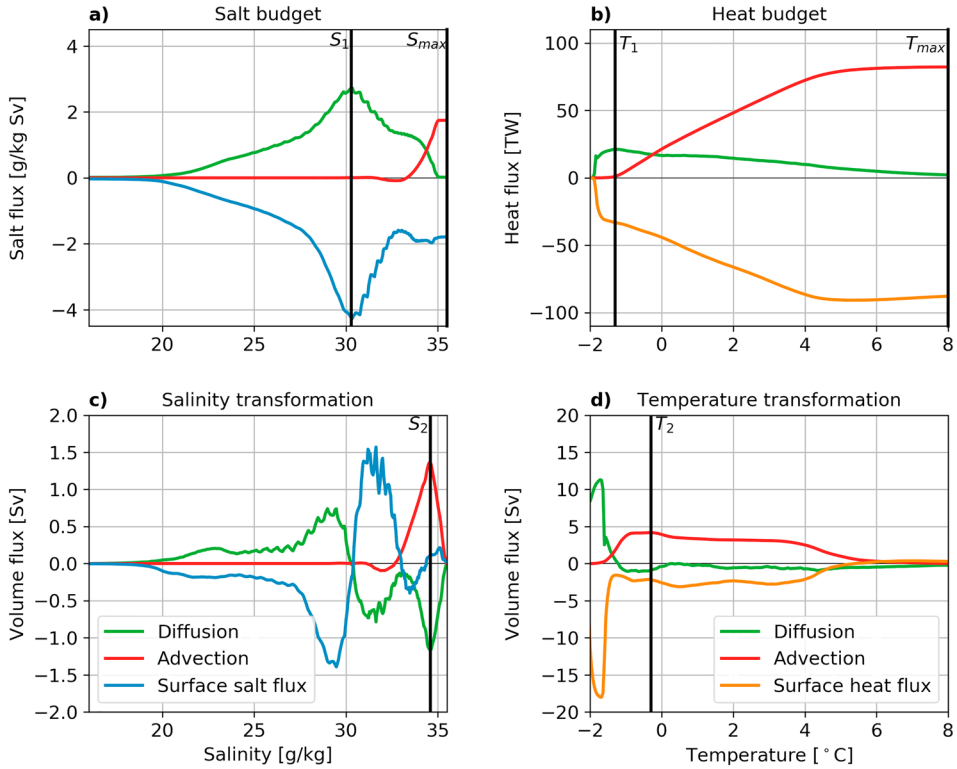

Figure 4. Model control water mass transformation. Panels (a) and (c) visualize Arctic salinity transformation; panels (b) and (d) visualize temperature transformation. The physical interpretation of the different lines is noted in the schematic graphs in Figures 3c–3f. Note that the lines in panels (c) and (d) are the derivatives of the lines in panels (a) and (b) with respect to salinity or temperature, respectively. S_1 and T_1 mark the isohaline and isotherm across, which salt and heat diffusion are maximum. S_{max} and T_{max} mark the maximum salinity and temperature in the model Arctic and are used for computing the total Arctic salt and heat budgets. S_2 and T_2 mark the difference between net inflows and outflows across the Arctic gateways and hence the maximum transformation of inflowing waters.

freshwater export across the Arctic gateways. The salt budget can thus be interpreted as a total freshwater budget in the Arctic.

The diffusion of salt necessarily transports salt from saline layers to fresh layers, as marked by the positive diffusive salt flux. The maximum salt diffusion crosses the isohaline marked by S_1 (Figure 4a). As this isohaline is fresher than all inflows and outflows across the Arctic gateways, this diffusive salt flux cannot be balanced by advection. Rather, it is balanced by the integrated negative surface salt flux into outcropping waters with a salinity below S_1. Diffusion in the model is the sum of isoneutral and diapycnal diffusion. As can be seen by the balance between diffusion and the surface salt flux across S_1, not all diffusion in the model is captured by these two diffusive terms. It should be noted that Gent-McWilliams fluxes are neglected in the present study, though these are small, in agreement with Pemberton et al. (2015), and cannot account for the missing diffusion.

The Arctic-wide heat budget (Figure 4b) qualitatively resembles the salt budget and is a balance between the integrated heat advection and surface heat fluxes below T_{max}. Not surprisingly, the heat advection across the Arctic gateways is positive and is balanced by a net surface heat loss. Similar to salt diffusion, there exists an isotherm T_1, which marks the maximum diffusive heat flux. This heat flux into cold waters with a temperature below T_1 is balanced by a net surface heat loss from the outcrop of these cold waters. Note that, again, diffusion of heat is underestimated and the isoneutral and diapycnal diffusion do not fully account for the total model diffusion.

The net salt advection into the Arctic is governed by a net inflow of relatively saline waters and a net outflow of fresher waters. The slope in advection indicates the net inflow and outflow of water of different salinities (Figure 4c): A negative (positive) slope indicates a net inflow (outflow) in a given salinity class (see also Figure 3e). In the model simulations, this transformation of a saline inflow to a fresher outflow is maximum

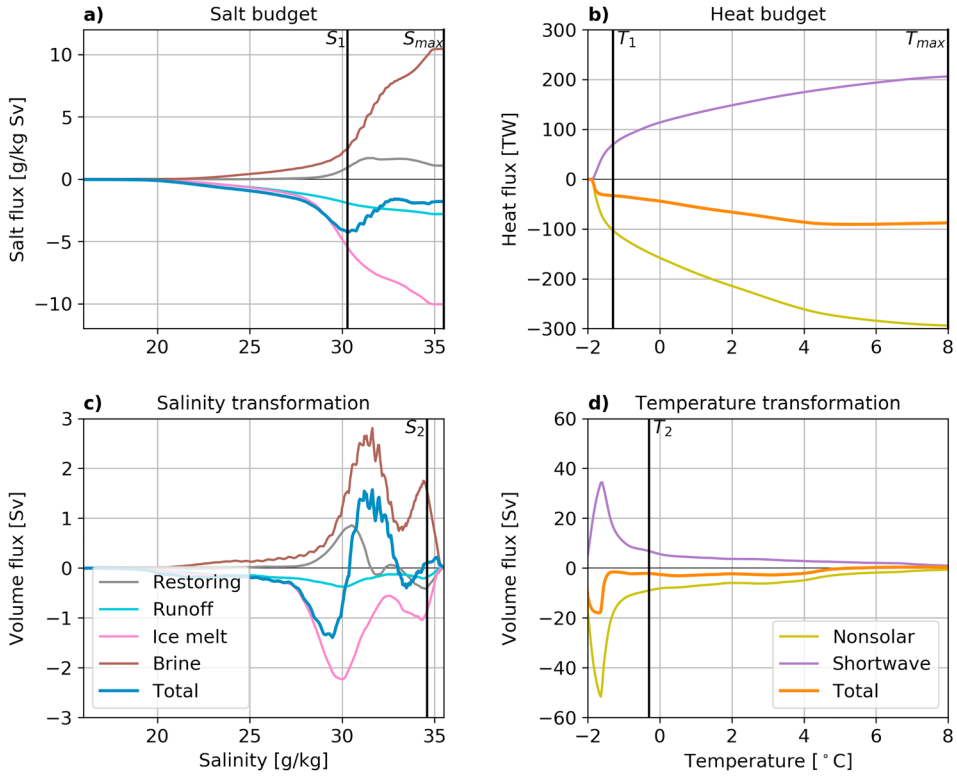

Figure 5. As in Figure 4 for the individual surface fluxes of salt and heat. The total surface fluxes (blue for salt and orange for heat) are identical to those in Figure 4.

across isohaline S_2 (Figure 4c). This transformation primarily describes the transformation of Atlantic Water entering through the Barents Sea and Fram Strait (see Figure 1a). We find that the freshening of Atlantic Water is predominantly governed by diffusion, indicating a small impact of direct surface freshening. This dominant diffusive freshening likely reflects a subduction of the Atlantic inflow below fresh surface layers (e.g., Rudels et al., 2015), which shelter the Atlantic Water from direct surface salt fluxes.

Besides the net inflow of Atlantic Water with a salinity above S_2, we can distinguish a fresh inflow between salinities 31 and 32 g/kg. This inflow, which undergoes net salinification within the Arctic Ocean, likely originates from the relatively fresh North Pacific. The salinification of this Pacific Water is governed by surface salt fluxes. This transformation is model specific and deviates from that presented by Pemberton et al. (2015). Because this salinification of Pacific Water is relatively small and model specific, we will not analyze this transformation in more depth.

The transformation of inflowing waters in terms of temperature is marked by a maximum cooling across isotherm T_2 (Figure 4d). This transformation represents the cooling of the Atlantic inflow as well as the relatively warm Pacific inflow during summer. The cooling of these inflowing waters is governed by both surface heat loss and diffusion. Although the latter appears small, this may be partly due to the underestimation of diffusion.

3.2. Surface Fluxes

The surface fluxes of (virtual) salt and heat in Figure 4 are composed of a number of separate physical terms. In Figure 5, we extract these separate terms that induce a net salt extraction and freshening, as well as net heat extraction and cooling of Arctic surface waters.

Surface salt fluxes are dominated by ice melt, brine rejection, river runoff, and a restoring term. Direct evaporation from and precipitation into the open ocean is small due to the large sea ice cover. Although net precipitation over the Arctic is considerable, the bulk falls on top of sea ice. As a result, it is either directly transported out of the Arctic through sea ice export, or it enters the Arctic Ocean indirectly through sea ice melt. The balance between the total ice melt and brine rejection ($S_{\max}$ in Figure 5a) suggests a net balance between sea ice export and net precipitation over sea ice, in agreement with considerations by Rudels (2015).

The total surface salt flux in the model is completed by a correction term to conserve salt globally, which is also negligible.

Over the complete salinity range, sea ice melt, and brine rejection dominate both the salt fluxes (Figure 5a) and the salinity transformation (Figure 5c). As described by Abernathey et al. (2016), sea ice melt occurs during summer when surface waters are relatively fresh, and brine rejection occurs during winter when surface waters are more saline. This seasonal asymmetry induces a net salt flux toward waters of high salinity. In addition, brine penetration transforms deeper and saltier layers, amplifying the net salt flux due to ice formation and melt. This salt flux dominates the maximum total surface salt flux across S_1, which is balanced by the maximum diffusive salt flux. Besides this redistribution of salt within the Arctic, sea ice processes have a minimal impact on the total salt budget (S_{max} in Figure 5a).

The total salt budget is governed by a negative (virtual) salt flux due to river runoff, and a smaller positive restoring salt flux. This restoring salt flux acts as a net source of salt, or equivalently as a net sink of freshwater, to compensate for a fresh bias in the model. As discussed by Ilıcak et al. (2016), the model used by Pemberton et al. (2015), NEMO3.2 with LIM2 sea ice component, has a saline bias over the Eurasian shelves. In their model, surface salinity restoring acts as a net sink of salt. These differences in salinity restoring between the two models affect the net salt advection across the Arctic gateways, which is a factor 2 larger in the model by Pemberton et al. (2015) compared to our simulations. This model-dependent salinity restoring likely reflects differences in the representation of the inflow of Atlantic Water between the two models.

In addition to acting as a net source of salt, the restoring salt flux acts as a horizontal diffusion by salinifying fresh layers and freshening saline layers, as indicated by the peak in Figure 5a. This horizontal diffusion indicates that horizontal salinity gradients in the model are larger than in the climatology to which surface salinity is restored, which either reflects a model bias with overestimated salinity gradients or reflects a climatology that is too smooth.

The surface salinity transformation across S_2 (Figure 5c), which marks the maximum freshening of Atlantic Water, is small, indicating that surface freshening is minimal. We see that this results from an overall balance in the salinity transformation due to brine rejection on one hand and ice melt, runoff, and restoring on the other hand.

As may be expected, the total surface heat flux is composed of two opposite terms: a positive heat flux from shortwave radiation and a negative nonsolar heat flux. As the latter dominates, the total surface heat flux is negative over the complete temperature range and induces a net surface cooling throughout the Arctic. The slight exception is the warmest water (above 5 ° C), which is only present during summer when shortwave warming dominates over nonsolar heat loss. This net warming is balanced by diffusive cooling (Figure 4d). Because the heat flux associated with this summer warming is relatively small, we will not analyze this feature in more detail.

3.3. Major Processes

The long-term mean Arctic water mass transformation can be summarized in terms of the balances across isohalines S_1 and S_2 and the isotherms T_1 and T_2. These balances are indicated in Figure 6.

The basin-wide Arctic salt budget is governed by a net salt import through the circulation and modification of Atlantic Water and a surface (virtual) salt extraction from the freshest waters; these are primarily shelf waters near river outlets. These salt fluxes are connected through a maximum salt diffusion across S_1. One can interpret this salt budget in terms of a freshwater transport in the opposite direction: River outlets feed freshwater into low salinity shelf waters. This freshwater diffuses into more saline layers where it mixes with the saline Atlantic inflow and is eventually exported from the Arctic as part of modified Atlantic Water.

In addition, the seasonal asymmetry between ice melt and brine rejection acts to increase near-surface salinity gradients by transporting salt into saline layers. This salt transport is balanced by an oppositely directed diffusive salt flux.

The basin-wide Arctic heat budget is governed by a net heat import from the Atlantic inflow and to a lesser extent the warm summer Pacific inflow. This heat import is partly balanced by a direct surface heat loss from the same warm waters and partly by a surface heat loss from cold outcropping layers. The heat flux from warm inflowing waters to cold outcropping waters is governed by an internal heat diffusion.

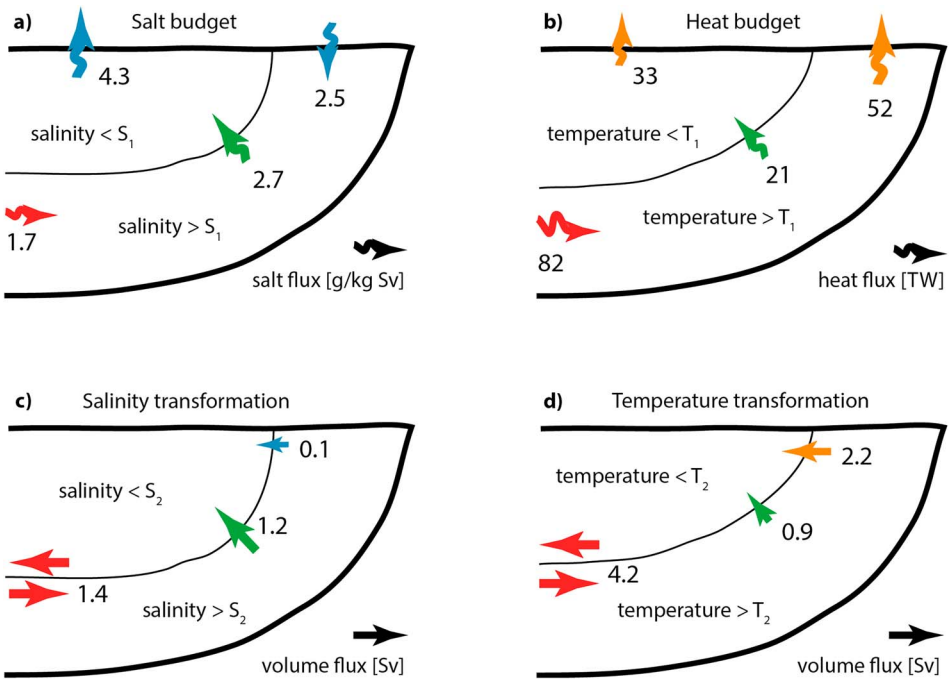

Figure 6. Illustration of major processes in the model control simulation. (a, b) The salt (heat) budget is described by dividing the Arctic into waters below and above the isohaline S_1 (isotherm T_1), which is defined by the maximum diffusion. (c, d) The salinity (temperature) transformation is described by dividing the Arctic into waters below and above the isohaline S_2 (isotherm T_2), which is defined by the maximum inflow transformation. Colors indicate the processes as in Figures 3a and 3b (red: advection, green: diffusion, blue: surface salt fluxes, orange: surface heat fluxes). Note that this illustration does not represent actual stratification or geographical features; it also does not explicitly distinguish between inflows and outflows across the different gateways. The inflows and outflows in panels (c) and (d) are of equal magnitude as prescribed by volume conservation. The residual of the three terms can be interpreted as an additional, unresolved diffusion, which is not shown.

4. Imprint of Runoff Variability

In order to understand the impact of runoff variability on Arctic water mass transformation, we study the perturbation of the control state due to a 30% increase in Arctic-wide river runoff. This perturbation is characterized by an equilibrium response and a response time scale, which both may vary throughout the season. As a first impression of the impact of increased runoff, it is insightful to analyze the change in sea surface hydrography, which is shown in Figure 7.

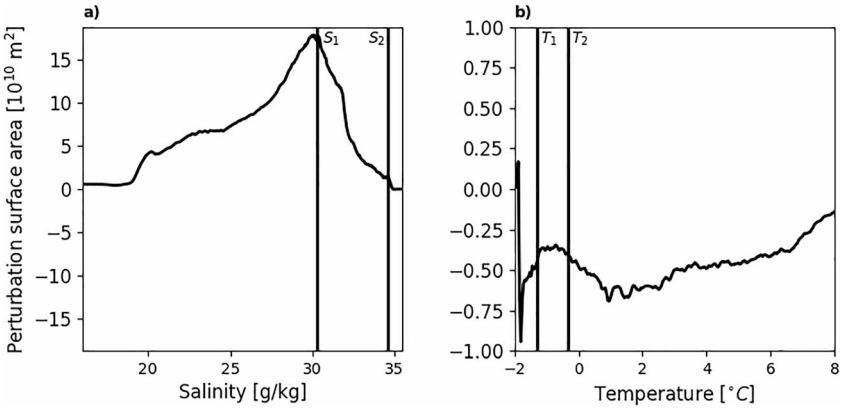

Figure 7. Change in sea surface hydrography due to increased runoff. (a) Perturbation of the annual mean cumulative surface area as a function of salinity; positive values indicate a net freshening. (b) Perturbation of the cumulative surface area in terms of temperature; negative values indicate a net warming. Note that not the full temperature range is shown, and a fraction of water is transformed to temperatures above 8 ° C.

Not surprisingly, there is an overall freshening of the Arctic sea surface after adjustment to the runoff increase. This freshening results in an overall increase in the outcrop of waters with a salinity below S_1. The adjustment of sea surface temperature is less trivial. Overall, there is a shift of surface waters toward higher temperatures, reflecting an overall warming of the Arctic sea surface due to increased river runoff. In particular, there is a decrease of surface waters at freezing point (negative peak in Figure 7b). A significant fraction of this sea surface is warmed to temperatures above 1 ° C, implying that the total surface area of waters below both T_1 and T_2 decreases.

4.1. Salt and Heat Budgets

The total Arctic salt budget in the control simulation is dominated by a balance between a salt influx from advection and surface restoring and a virtual salt extraction by river runoff (S_{max} in Figures 4a and 5a). In addition, there is a near-balance between a salt influx by brine rejection and a virtual salt extraction by sea ice melt. The 30% perturbation in runoff prescribes an increase in the virtual salt extraction due to runoff (Figure 8a). In the model, this perturbation induces an increased salt influx into the Arctic by restoring and advection. The model-specific restoring response balances 80% of the perturbation, indicating that the physically realistic model response is damped. In absence of this restoring salt flux, the increase in salt import (or equivalently freshwater export) would therefore be a factor 5 larger in order to restore balance. This increased salt import could either come from a magnified response in salt advection, an increase in net sea ice export, or some combination of both. In our simulations, we find a limited response in sea ice export, which would be expressed by an uneven response between ice melt and brine rejection. It is therefore likely that the response in total salt advection is damped by an approximate factor of 5 due to salinity restoring.

The total Arctic heat budget in the control simulation is described by a balance between heat import through advection and shortwave heating, and net heat loss by the nonsolar surface heat flux (T_{max} in Figures 4b and 5b). The decreased sea ice cover increases the net incoming shortwave heat flux into the Arctic surface waters (Figure 8b). Additionally, the net outgoing nonsolar heat flux increases as may be expected from a decreased sea ice cover and an overall increased sea surface temperature. The increased nonsolar heat flux dominates over the increased incoming shortwave heat flux, leading to an increase in the total net surface heat loss. This surface heat loss is balanced by an increase in the advective heat import across the gateways, in agreement with comparable model studies where Arctic runoff is increased by 30% (Nummelin et al., 2016; Pemberton & Nilsson, 2016).

In the control simulation, a maximum diffusive salt flux is found across S_1, balanced by a net salt extraction from the surface outcrop layers with a salinity below S_1. This surface salt extraction is dominated by runoff and sea ice melt, partly suppressed by the restoring salt flux and brine rejection (S_1 in Figures 4a and 5b). The runoff perturbation primarily increases the balance between salt diffusion, salinity restoring, and runoff (Figure 8c). In addition, the increased outcrop of waters with a salinity below S_1 results in an increase in sea ice melt and brine rejection into these fresh layers.

Finally, a similar maximum heat diffusion was found in the control simulation across T_1, balanced primarily by a net surface heat loss dominated by the nonsolar heat loss over the incoming shortwave heat flux (T_1 in Figures 4b and 5b). As indicated by Nummelin et al. (2015), increased runoff suppresses mixing by increasing the stratification, but it also increases the vertical temperature gradient by warming the Atlantic layer. These opposing effects can either increase or decrease heat diffusion, and in our model results, the positive runoff perturbation increases the maximum diffusion across T_1 (Figure 8d). This increased vertical heat flux likely causes the surface warming, which induces an increase in nonsolar heat loss and a decrease in the sea ice cover. Note that this response can only occur if there is a sufficient temperature gradient across the halocline. In the real Arctic, this effect may only be expected to occur in the Eurasian basin, as the Canadian basin hosts a cold halocline (Rudels et al., 1996; Steele & Boyd, 1998). As our model has a cold bias at depth and underestimates the vertical temperature gradient across the halocline, the increase in heat import and surface heat loss to increased runoff may be underestimated as well.

4.2. Salinity and Temperature Transformation

The increase in runoff is necessarily balanced by a net salt import or equivalently by a net freshwater export. Although the model resolves a large fraction of this freshwater export through an enhanced restoring salt flux, the realistic response by advection is present as well (Figure 8a). This response of enhanced advective freshwater export can be resolved either by an increased outflow of low-salinity waters or by an increased transformation of the inflowing waters. The first would imply a direct balance between surface fluxes and

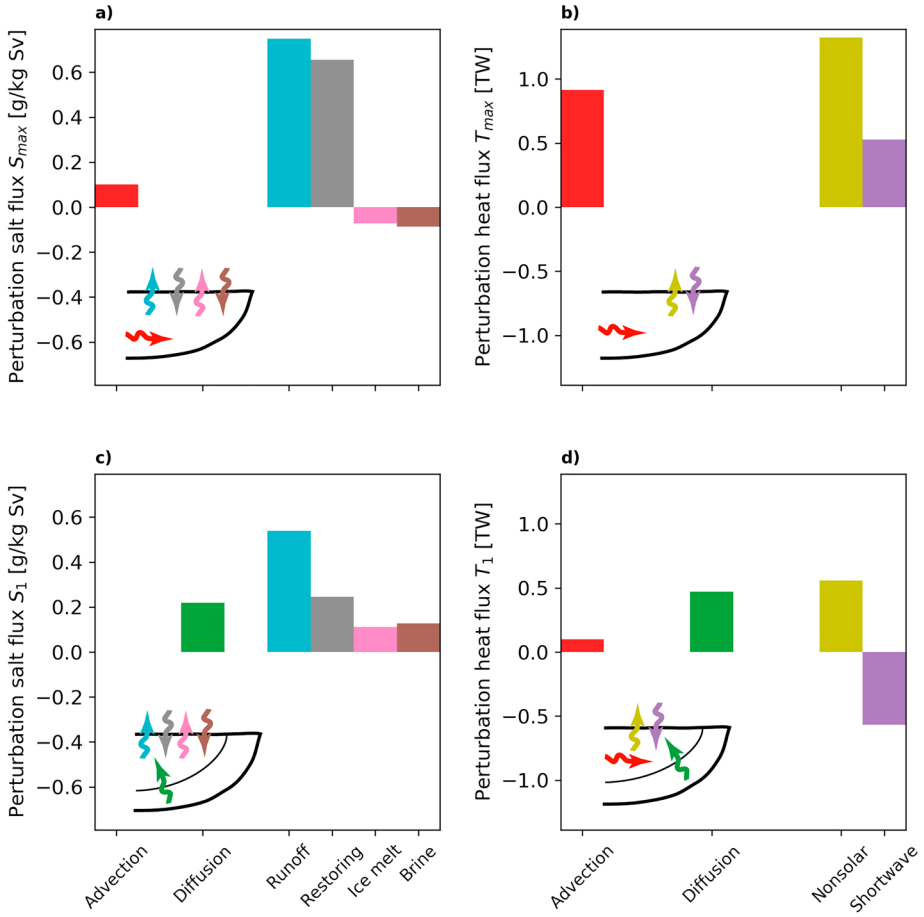

Figure 8. Equilibrium response of salt and heat fluxes to 30% increase in river runoff. The insets indicate the direction of each salt or heat flux in the control state. Positive (negative) perturbations indicate in increase (decrease) of these control fluxes. (a) Total salt budget marked by $S_{\max}$. (b) Total heat budget marked by $T_{\max}$. (c) Salt budget in waters with a salinity below S_1, which equals the balance of the maximum salt diffusion. (d) Heat budget in waters with a temperature below T_1, which equals the balance of the maximum heat diffusion.

advection in the freshest layers; the latter requires the downward diffusion of freshwater into the circulating water masses.

We find that, in the model, increased runoff is partly diffused into more saline layers. This directly impacts the maximum freshening of inflowing waters (Figure 9a). Direct surface freshening of inflowing waters, however, remains largely constant. Increased freshening through runoff, and suppressed salinification through brine rejection, is largely compensated by a reduced freshening due to surface salinity restoring.

The runoff perturbation also impacts the temperature transformation of inflowing waters. Direct surface cooling is suppressed due to increased shortwave warming and decreased cooling due to nonsolar heat loss (Figure 9b). However, the increased diffusive cooling dominates in the transformation of waters of temperature T_2. As a result, the inflowing waters are cooled more intensively when more runoff enters the Arctic.

4.3. Transient Imprint of Runoff

The aim of this paper is to quantify the transient imprint of runoff on Arctic water mass transformation. This transient imprint is outlined in Table 1, in which the dominant perturbations, as shown in Figures 8 and 9, are presented chronologically dependent on the associated adjustment time scales. Because these time scales τ_s vary between calendar months, we present the range of time scales for the months in which the sensitivity δ_s is significant.

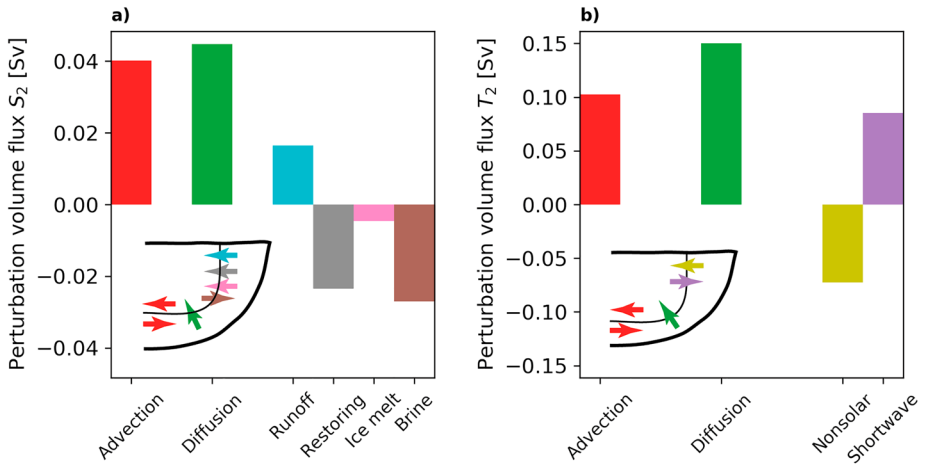

Figure 9. Equilibrium response of the maximum transformation of inflowing waters to 30% increase in river runoff. (a) The maximum salinity transformation marked by S_2. (b) The maximum temperature transformation marked by T_2. The insets indicate the direction of each volume flux in the control state. Positive (negative) perturbations indicate an increase (decrease) of these control fluxes.

Besides this chronological ordering of model responses to runoff increase, we present three quantitative measures for the magnitude of the response and the skill of the sCRF. The signal-to-noise ratio is the magnitude of the perturbation, divided by the standard deviation of the associated salt, heat, or volume flux in the control simulation; this ratio is a measure for the significance of the perturbation. The goodness of fit for the sCRF is the explained variance of the modeled adjustment to the step function increase in runoff by the idealized sCRF; this goodness of fit is a measure for the appropriateness of the exponential fit. Finally, the explained model variance is the percentage of the modeled variance by the reconstructed time series based on the sCRF and the time series of the variable Arctic runoff; this value is a measure for the potential predictability of Arctic water mass processes based on river runoff.

For several water mass transformation processes, a relatively large fraction of the variance can be explained by the variability in total Arctic river runoff through application of the sCRF. These processes include freshwater diffusion and the year-to-year variations in sea ice formation and melt. On longer time scales, the variability in the freshening of Atlantic Water and the total Arctic freshwater export can also be partly explained by runoff variability. These results reveal that the sCRF can potentially be used to predict a fraction of the variability of Arctic water mass transformation processes several years ahead in time.

Table 1
Chronological Model Response to Runoff Perturbations and Quantification of the Seasonal CRF Performance

Model response	Adjustment time scale τ_s (years)	Signal-to-noise ratio	Goodness of CRF fit (%)	Explained model variance (%)
Downward freshwater diffusion increases	0.3–0.5	24	57	53
Restoring salt flux increases	0.8–1.2	97	98	72
Total sea ice melt decreases	0.6–1.8	7	70	27
Total brine rejection decreases	1.5–1.8	9	78	34
Shortwave surface warming increases	2–4	3	35	4
Freshening of Atlantic inflow increases	2–4	1.3	19	27
Total freshwater export increases	2.5–4	2.7	45	28
Nonsolar surface heat loss increases	1–5	2.7	29	7
Maximum heat diffusion increases	2.5–7	1.5	18	7
Total heat import increases	5–10	1.3	18	20

Note. CRF = climate response function.

5. Discussion

A number of studies have previously estimated response time scales associated with perturbations in Arctic river runoff. Based on the observed total freshwater input and freshwater storage, Haine et al. (2015) and Carmack et al. (2016) found a residence time of approximately 15 years. Using passive tracers, Pemberton et al. (2014) found a residence time of 10 years for freshwater from Eurasian rivers. These estimates agree well with our simulations, which give an exponential time scale of up to 4 years for total freshwater export, implying that 95% of a runoff perturbation exits the Arctic within 12 years. However, Jahn, Tremblay, Newton, et al. (2010) noted that residence times of runoff may be significantly reduced by favorable atmospheric conditions. Using idealized simulations, Manucharyan and Spall (2016) showed that eddies may play an important role in regulating the impact of atmospheric conditions on the residence times of freshwater. Because the time scales reported in this study are based on mean atmospheric conditions, the actual response time scales to variability in Arctic river runoff likely contain a considerable spread.

We find that surface salinity restoring significantly impacts salinity transformation in the control simulation and has an even greater impact on the response to runoff variability. In part, we interpret this as an overall damping of the perturbation by an approximate factor of 5. However, this interpretation is insufficient with regard to the transient response to perturbations due to the considerable adjustment time scale of the restoring salt flux. As the adjustment time scales of the total restoring salt flux are up to 1.2 years, the transient impact of runoff may be larger during the first years after a perturbation. As salt diffusion responds on shorter time scales than restoring, the response of diffusion might—at least temporarily—be significantly stronger than expected from the apparently damped runoff perturbation. Altogether, the complications introduced by surface salinity restoring suggest that the transient response to runoff variability may vary greatly between uncoupled models. This impact of salinity restoring can be suppressed either by masking restoring within the region of interest (e.g., Nummelin et al., 2016) or by performing fully coupled simulations.

The explained model variance of several processes related to Arctic salinity and temperature transformation is considerable (Table 1), though it is limited by a number of factors. First, a weak sensitivity to runoff perturbations with respect to internal variability can suppress the explained model variance. Second, the idealized shape of the CRF, an exponential decay function, may not sufficiently describe the response to perturbations. This limitation may be caused by nonlinearity or by an interaction between the different terms. Note that the method presented here can be expanded by a more general CRF formulation to improve its functionality. Finally, we have considered total Arctic runoff as the governing parameter, neglecting any spatiotemporal variability in runoff. Such variability could, for example, be induced by an anticovariance between runoff from the Canadian and Eurasian rivers. Despite these limiting factors and the relatively small perturbation of 30% runoff, we find a considerable explained model variance due to total Arctic runoff, primarily for salinity transformation processes.

6. Conclusions

In this paper, we determine the transient response of Arctic salinity and temperature transformation to variability in Arctic river runoff using a global coupled ocean-sea ice model. From this response we quantify the explained model variance of Arctic water mass transformation from runoff variability.

A stepwise increase in runoff sets off a chain of events with a range of time scales from several months up to 10 years. Initially, the freshening of shelf waters induces an increase in the downward diffusion of freshwater into deeper layers within half a year after the perturbation. The freshening of surface waters further induces an increased restoring salt flux on a time scale of 1 year. Within 2 years after the perturbation, the sea ice cover has shrunk, leading to a reduced seasonal cycle of sea ice formation and melt. On a time scale of several years, the surface warming due to shortwave radiation increases, likely due to the decreased sea ice extent, and the freshening of inflowing Atlantic Water increases, likely due to the downward diffusion of freshwater. The total freshwater export increases at a time scale up to 4 years, restoring the total freshwater budget in the Arctic. Finally, on time scales up to 10 years, the heat budget in the Arctic adjusts, which can be summarized by an increase in advective heat import, heat diffusion, and surface heat loss.

The response of surface salinity restoring dominates the anomalous salinity transformation in the Arctic, and after full adjustment, it compensates 80% of the runoff perturbation. As a result, only 20% of the runoff

perturbation contributes to enhanced Arctic freshwater export. This implies that the model's dynamical response to runoff variability is strongly damped. In addition, the surface salinity restoring in the control simulation is found to be strongly model dependent, as it compensates model biases. The large differences in salinity restoring between models indicate that the magnitude of the dynamical response to runoff variability may also be model dependent.

The imprint of runoff variability on Arctic water mass transformation is quantified using seasonal climate response functions. These describe an idealized response to runoff perturbations, which is compared to the variability in water mass transformation in actual model simulations, forced by variable Arctic river runoff. The considerable explained model variance for several processes, including the decrease in sea ice melt and brine rejection, indicate the potential for predictability of Arctic processes based on river runoff several years ahead. It should be noted here that these simulations do not contain interannual forcing beyond Arctic river runoff, and the actual predictability of the real system is likely smaller due to variability from other sources such as the Arctic Oscillation.

The increase in salt diffusion in response to increased runoff eventually induces an increase in heat diffusion. This response is likely limited to the Eurasian basin where significant temperature gradients are present across the halocline. As a result, increased runoff strengthens the heat advection into the Arctic, as well as the surface heat loss. The response of increased diffusion and advection of both salt and heat hints to an overall spinup of the Arctic estuarine circulation, although the response in total volume exchange across the gateways is not analyzed explicitly. As the model response of temperature transformation is relatively small compared to internal variability, the explained model variance of temperature transformation is limited. However, the model may underestimate the response in the circulation of heat due to the aforementioned salinity restoring and due to a cold bias below the halocline.

Overall, our findings provide encouraging evidence for the potential predictability of the Arctic system based on variability in river runoff. More generally, they illustrate the application of the seasonal climate response function. This novel tool allows for the quantification of transient climate responses on monthly resolution. Although this is particularly relevant for the Arctic, as it has a strong seasonality and a large fraction of variability is rapid because it is constrained to the upper layers of the ocean, we suggest that the seasonal climate response function can be applied to the analysis of any regional climate system, which is subject to a strong seasonality.

Acknowledgments
We thank I. Bethke and M. Bentsen for help with implementing online diagnostics into MICOM. E. L. and M. I. are funded by the Norwegian Research Council project NORTH; P. P. is funded by NordForsk project Nordic Center of Excellence Arctic Climate Prediction: Pathways to Resilient, Sustainable Societies (ARCPATH) (Grant 76654). M. I. is also partially funded by ITU-TGA-2017-40657 and ITU Polar Research Center (PolRec). As part of the work, P. P. received a Bjerknes visiting fellowship from the Bjerknes Centre. Processed data used for the figures and computations are available at https://doi.org/10.5281/zenodo.1886889. The idea to use CRFs arose at the 2016 FAMOS workshop during a meeting of the CRF-working group led by J. Marshall. We are grateful for detailed comments by M. Muilwijk and T. Eldevik that helped shape paper. Finally, we thank S. Groeskamp, three anonymous reviewers, and the Editor for very useful comments that greatly improved the paper.

References

Abernathey, R. P., Cerovecki, I., Holland, P. R., Newsom, E., Mazloff, M., & Talley, L. D. (2016). Water-mass transformation by sea ice in the upper branch of the southern ocean overturning. *Nature Geoscience*, *9*(8), 596–601. https://doi.org/10.1038/ngeo2749

Anderson, L. G., Jutterström, S., Kaltin, S., Jones, E. P., & Björk, G. (2004). Variability in river runoff distribution in the Eurasian Basin of the Arctic Ocean. *Journal of Geophysical Research*, *109*, C01016. https://doi.org/10.1029/2003JC001773

von Appen, W.-J., Schauer, U., Hattermann, T., & Beszczynska-Möller, A. (2016). Seasonal cycle of mesoscale instability of the West Spitsbergen Current. *Journal of Physical Oceanography*, *46*(4), 1231–1254.

Årthun, M., Eldevik, T., Smedsrud, L. H., Skagseth, Ø., & Ingvaldsen, R. (2012). Quantifying the influence of Atlantic heat on Barents Sea ice variability and retreat. *Journal of Climate*, *25*(13), 4736–4743.

Badin, G., & Williams, R. G. (2010). On the buoyancy forcing and residual circulation in the Southern Ocean: The feedback from Ekman and eddy transfer. *Journal of Physical Oceanography*, *40*(2), 295–310. https://doi.org/10.1175/2009JPO4080.1

Badin, G., Williams, R. G., Jing, Z., & Wu, L. (2013). Water mass transformations in the Southern Ocean diagnosed from observations: Contrasting effects of air-sea fluxes and diapycnal mixing. *Journal of Physical Oceanography*, *43*(7), 1472–1484. https://doi.org/10.1175/JPO-D-12-0216.1

Bauch, D., Schlosser, P., & Fairbanks, R. G. (1995). Freshwater balance and the sources of deep and bottom waters in the Arctic Ocean inferred from the distribution of $H_2^{18}O$. *Progress in Oceanography*, *35*(1), 53–80. https://doi.org/10.1016/0079-6611(95)00005-2

Bentsen, M., Bethke, I., Debernard, J., Iversen, T, Kirkevåg, A, Seland, Ø., et al. (2013). The Norwegian earth system model, NorESM1-M-Part 1: Description and basic evaluation of the physical climate. *Geoscientific Model Development*, *6*(3), 687–720.

Bitz, C., Fyfe, J. C., & Flato, G. M. (2002). Sea ice response to wind forcing from AMIP models. *Journal of Climate*, *15*(5), 522–536.

Bleck, R., & Smith, L. T. (1990). A wind-driven isopycnic coordinate model of the north and equatorial Atlantic Ocean: 1. Model development and supporting experiments. *Journal of Geophysical Research*, *95*(C3), 3273–3285.

Carmack, E. C., Yamamoto-Kawai, M., Haine, T. W. N., Bacon, S., Bluhm, B. A., Lique, C., et al. (2016). Freshwater and its role in the Arctic Marine System: Sources, disposition, storage, export, and physical and biogeochemical consequences in the Arctic and global oceans. *Journal of Geophysical Research: Biogeosciences*, *121*, 675–717. https://doi.org/10.1002/2015JG003140

Danabasoglu, G., Yeager, S. G., Kim, W. M., Behrens, E., Bentsen, M., Bi, D., et al. (2016). North Atlantic simulations in Coordinated Ocean-ice Reference Experiments phase II (CORE-II). Part II: Inter-annual to decadal variability. *Ocean Modelling*, *97*, 65–90. https://doi.org/10.1016/j.ocemod.2015.11.007

Delworth, T. L., & Zeng, F. (2016). The impact of the North Atlantic Oscillation on climate through its influence on the Atlantic Meridional Overturning Circulation. *Journal of Climate*, *29*(3), 941–962. https://doi.org/10.1175/JCLI-D-15-0396.1

Déry, S. J., & Wood, E. F. (2004). Teleconnection between the Arctic Oscillation and Hudson Bay river discharge. *Geophysical Research Letters*, *31*, L18205. https://doi.org/10.1029/2004GL020729

Döös, K., Nilsson, J., Nycander, J., Brodeau, L., & Ballarotta, M. (2012). The World Ocean thermohaline circulation. *Journal of Physical Oceanography*, *42*(9), 1445–1460. https://doi.org/10.1175/JPO-D-11-0163.1

Eldevik, T., & Nilsen, J. E. Ø. (2013). The Arctic–Atlantic thermohaline circulation. *Journal of Climate*, *26*(21), 8698–8705.

Grist, J. P., Josey, S. A., Zika, J. D., Evans, D. G., & Skliris, N. (2016). Assessing recent air-sea freshwater flux changes using a surface temperature-salinity space framework. *Journal of Geophysical Research: Oceans*, *121*, 8787–8806. https://doi.org/10.1002/2016JC012091

Groeskamp, S., Sloyan, B. M., Zika, J. D., & McDougall, T. J. (2017). Mixing inferred from an ocean climatology and surface fluxes. *Journal of Physical Oceanography*, *47*(3), 667–687. https://doi.org/10.1175/JPO-D-16-0125.1

Groeskamp, S., & Iudicone, D. (2018). The effect of air– sea flux products, shortwave radiation depth penetration, and albedo on the upper ocean overturning circulation. *Geophysical Research Letters*, *45*, 9087–9097. https://doi.org/10.1029/2018GL078442

Groeskamp, S., Zika, J. D., McDougall, T. J., Sloyan, B. M., & Laliberté, F. (2014). The representation of ocean circulation and variability in thermodynamic coordinates. *Journal of Physical Oceanography*, *44*(7), 1735–1750. https://doi.org/10.1175/JPO-D-13-0213.1

Groeskamp, S., Zika, J. D., Sloyan, B. M., McDougall, T. J., & McIntosh, P. C. (2014). A thermohaline inverse method for estimating diathermohaline circulation and mixing. *Journal of Physical Oceanography*, *44*(10), 2681–2697. https://doi.org/10.1175/JPO-D-14-0039.1

Guemas, V., Blanchard-Wrigglesworth, E., Chevallier, M., Day, J. J., Déqué, M., Doblas-Reyes, F. J., et al. (2016). A review on Arctic sea-ice predictability and prediction on seasonal to decadal time-scales. *Quarterly Journal of the Royal Meteorological Society*, *142*(695), 546–561. https://doi.org/10.1002/qj.2401

Haine, T. W., Curry, B., Gerdes, R., Hansen, E., Karcher, M., Lee, C., et al. (2015). Arctic freshwater export: Status, mechanisms, and prospects. *Global and Planetary Change*, *125*, 13–35.

Hasselmann, K., Sausen, R., Maier-Reimer, E., & Voss, R. (1993). On the cold start problem in transient simulations with coupled atmosphere-ocean models. *Climate Dynamics*, *9*(2), 53–61.

Hattermann, T., Isachsen, P. l. E., von Appen, W.-J., Albretsen, J., & Sundfjord, A. (2016). Eddy-driven recirculation of Atlantic Water in Fram Strait. *Geophysical Research Letters*, *43*, 3406–3414. https://doi.org/10.1002/2016GL068323

Hieronymus, M., Nilsson, J., & Nycander, J. (2014). Water mass transformation in salinity-temperature space. *Journal of Physical Oceanography*, *44*(9), 2547–2568. https://doi.org/10.1175/JPO-D-13-0257.1

Huang, R. X. (1993). Real freshwater flux as a natural boundary condition for the salinity balance and thermohaline circulation forced by evaporation and precipitation. *Journal of Physical Oceanography*, *23*(11), 2428–2446.

Hunke, E. C., Lipscomb, W. H., Turner, A. K., Jeffery, N., & Elliott, S. (2010). CICE: the Los Alamos sea ice model documentation and software user's manual version 4.1 LA-CC-06-012 (*T-3 Fluid Dynamics Group*). USA: Los Alamos National Laboratory. 675.

Ilıcak, M., Drange, H., Wang, Q., Gerdes, R., Aksenov, Y., Bailey, D., et al. (2016). An assessment of the Arctic Ocean in a suite of interannual CORE-II simulations. Part III: Hydrography and fluxes. *Ocean Modelling*, *100*, 141–161.

Iudicone, D., Madec, G., & McDougall, T. J. (2008). Water-mass transformations in a neutral density framework and the key role of light penetration. *Journal of Physical Oceanography*, *38*, 1357–1376. https://doi.org/10.1175/2007JPO3464.1

Jahn, A., Tremblay, B., Mysak, L. A., & Newton, R. (2010). Effect of the large-scale atmospheric circulation on the variability of the Arctic Ocean freshwater export. *Climate Dynamics*, *34*(2), 201–222. https://doi.org/10.1007/s00382-009-0558-z

Jahn, A., Tremblay, L. B., Newton, R., Holland, M. M., Mysak, L. A., & Dmitrenko, I. A. (2010). A tracer study of the Arctic Ocean's liquid freshwater export variability. *Journal of Geophysical Research*, *115*, C07015. https://doi.org/10.1029/2009JC005873

Johnson, H. L., Cornish, S. B., Kostov, Y., Beer, E., & Lique, C. (2018). Arctic Ocean freshwater content and its decadal memory of sea-level pressure. *Geophysical Research Letters*, *45*, 4991–5001. https://doi.org/10.1029/2017GL076870

Kostov, Y., Ferreira, D., Armour, K. C., & Marshall, J. (2018). Contributions of greenhouse gas forcing and the Southern Annular Mode to historical southern ocean surface temperature trends. *Geophysical Research Letters*, *45*, 1086–1097. https://doi.org/10.1002/2017GL074964

Kostov, Y., Marshall, J., Hausmann, U., Armour, K. C., Ferreira, D., & Holland, M. M. (2017). Fast and slow responses of Southern Ocean sea surface temperature to SAM in coupled climate models. *Climate Dynamics*, *48*(5), 1595–1609. https://doi.org/10.1007/s00382-016-3162-z

Krahmann, G., & Visbeck, M. (2003). Arctic Ocean sea ice response to Northern Annular Mode-like wind forcing. *Geophysical Research Letters*, *30*(15), 1793. https://doi.org/10.1029/2003GL017354

Lambert, E., Eldevik, T., & Haugan, P. M. (2016). How northern freshwater input can stabilise thermohaline circulation. *Tellus A: Dynamic Meteorology and Oceanography*, *68*(1), 31051. https://doi.org/10.3402/tellusa.v68.31051

Large, W. G., & Yeager, S. G. (2004). Diurnal to decadal global forcing for ocean and sea–ice models: The data sets and flux climatologies. Boulder, Colorado: National Center for Atmospheric Research. (May), 105pp, https://doi.org/10.5065/D6KK98Q6

Large, W. G., & Yeager, S. (2009). The global climatology of an interannually varying air-sea flux data set. *Climate Dynamics*, *33*(2–3), 341–364.

Manucharyan, G. E., & Spall, M. A. (2016). Wind-driven freshwater buildup and release in the Beaufort Gyre constrained by mesoscale eddies. *Geophysical Research Letters*, *43*, 273–282. https://doi.org/10.1002/2015GL065957

Marshall, D. (1997). Subduction of water masses in an eddying ocean. *Journal of Marine Research*, *55*(2), 201–222. https://doi.org/10.1357/0022240973224373

Marshall, J., Jamous, D., & Nilsson, J. (1999). Reconciling thermodynamic and dynamic methods of computation of water-mass transformation rates. *Deep Sea Research Part I: Oceanographic Research Papers*, *46*(4), 545–572. https://doi.org/10.1016/S0967-0637(98)00082-X

Marshall, J., Scott, J., & Proshutinsky, A. (2017). "Climate response functions" for the Arctic Ocean: A proposed coordinated modelling experiment. *Geoscientific Model Development*, *10*(7), 2833–2848. https://doi.org/10.5194/gmd-10-2833-2017

Niederdrenk, A. L., Sein, D. V., & Mikolajewicz, U. (2016). Interannual variability of the Arctic freshwater cycle in the second half of the twentieth century in a regionally coupled climate model. *Climate Dynamics*, *47*(12), 3883–3900. https://doi.org/10.1007/s00382-016-3047-1

Nummelin, A., Ilicak, M., Li, C., & Smedsrud, L. H. (2016). Consequences of future increased Arctic runoff on Arctic Ocean stratification, circulation, and sea ice cover. *Journal of Geophysical Research: Oceans*, *121*, 617–637. https://doi.org/10.1002/2015JC011156

Nummelin, A., Li, C., & Smedsrud, L. H. (2015). Response of Arctic Ocean stratification to changing river runoff in a column model. *Journal of Geophysical Research: Oceans*, *120*, 2655–2675. https://doi.org/10.1002/2014JC010571

Nurser, A. J. G., Marsh, R., & Williams, R. G. (1999). Diagnosing water mass formation from air-sea fluxes and surface mixing. *Journal of Physical Oceanography*, *29*(7), 1468–1487. https://doi.org/10.1175/1520-0485(1999)029<1468:DWMFFA>2.0.CO;2

Onarheim, I. H., Eldevik, T., Årthun, M., Ingvaldsen, R. B., & Smedsrud, L. H. (2015). Skillful prediction of Barents Sea ice cover. *Geophysical Research Letters*, *42*, 5364–5371. https://doi.org/10.1002/2015GL064359

Pemberton, P., & Nilsson, J. (2016). The response of the central Arctic Ocean stratification to freshwater perturbations. *Journal of Geophysical Research: Oceans*, *121*, 792–817. https://doi.org/10.1002/2015JC011003

Pemberton, P., Nilsson, J., Hieronymus, M., & Meier, H. M. (2015). Arctic Ocean water mass transformation in S–T coordinates. *Journal of Physical Oceanography*, *45*(4), 1025–1050.

Pemberton, P., Nilsson, J., & Meier, H. M. (2014). Arctic Ocean freshwater composition, pathways and transformations from a passive tracer simulation. *Tellus A: Dynamic Meteorology and Oceanography*, *66*(1), 23988.

Peterson, B. J., Holmes, R. M., McClelland, J. W., Vörösmarty, C. J., Lammers, R. B., Shiklomanov, A. I., et al. (2002). Increasing river discharge to the Arctic Ocean. *Science*, *298*(5601), 2171–2173.

Rigor, I. G., Wallace, J. M., & Colony, R. L. (2002). Response of sea ice to the Arctic Oscillation. *Journal of Climate*, *15*(18), 2648–2663. https://doi.org/10.1175/1520-0442(2002)015<2648:ROSITT>2.0.CO;2

Rudels, B. (2010). Constraints on exchanges in the Arctic Mediterranean—Do they exist and can they be of use? *Tellus A*, *62*(2), 109–122.

Rudels, B. (2015). Arctic Ocean circulation, processes and water masses: A description of observations and ideas with focus on the period prior to the International Polar Year 2007–2009. *Progress in Oceanography*, *132*, 22–67. https://doi.org/10.1016/j.pocean.2013.11.006

Rudels, B, Anderson, L., & Jones, E. (1996). Formation and evolution of the surface mixed layer and halocline of the Arctic Ocean. *Journal of Geophysical Research*, *101*(C4), 8807–8821.

Rudels, B., Korhonen, M., Schauer, U., Pisarev, S., Rabe, B., & Wisotzki, A. (2015). Circulation and transformation of Atlantic water in the Eurasian Basin and the contribution of the Fram Strait inflow branch to the Arctic Ocean heat budget. *Progress in Oceanography*, *132*, 128–152. https://doi.org/10.1016/j.pocean.2014.04.003

Sloyan, B. M., & Rintoul, S. R. (2000). Estimates of area-averaged diapycnal fluxes from basin-scale budgets. *Journal of Physical Oceanography*, *30*(9), 2320–2341. https://doi.org/10.1175/1520-0485(2000)030<2320:EOAADF>2.0.CO;2

Sloyan, B. M., & Rintoul, S. R. (2001). The Southern Ocean limb of the global deep overturning circulation. *Journal of Physical Oceanography*, *31*(1), 143–173. https://doi.org/10.1175/1520-0485(2001)031<0143:TSOLOT>2.0.CO;2

Smedsrud, L. H., Sirevaag, A., Kloster, K., Sorteberg, A., & Sandven, S. (2011). Recent wind driven high sea ice area export in the Fram Strait contributes to Arctic sea ice decline. *The Cryosphere*, *5*, 821–829.

Speer, K. G. (1993). Conversion among North Atlantic surface water types. *Tellus A*, *45*(1), 72–79.

Speer, K., & Tziperman, E. (1992). Rates of water mass formation in the North Atlantic Ocean. *Journal of Physical Oceanography*, *22*(1), 93–104.

Steele, M., & Boyd, T. (1998). Retreat of the cold halocline layer in the Arctic Ocean. *Journal of Geophysical Research*, *103*(C5), 10,419–10,435.

Stigebrandt, A. (1985). On the hydrographic and ice conditions in the northern North Atlantic during different phases of a glaciation cycle. *Palaeogeography, Palaeoclimatology, Palaeoecology*, *50*(2-3), 303–321.

Tziperman, E. (1986). On the role of interior mixing and air-sea fluxes in determining the stratification and circulation of the oceans. *Journal of Physical Oceanography*, *16*(4), 680–693. https://doi.org/10.1175/1520-0485(1986)016<0680:OTROIM>2.0.CO;2

Van Hateren, J. (2013). A fractal climate response function can simulate global average temperature trends of the modern era and the past millennium. *Climate Dynamics*, *40*(11-12), 2651–2670.

Walin, G. (1977). A theoretical framework for the description of estuaries. *Tellus*, *29*(2), 128–136.

Walin, G. (1982). On the relation between sea-surface heat flow and thermal circulation in the ocean. *Tellus*, *34*(2), 187–195. https://doi.org/10.1111/j.2153-3490.1982.tb01806.x

Zika, J. D., England, M. H., & Sijp, W. P. (2012). The ocean circulation in thermohaline coordinates. *Journal of Physical Oceanography*, *42*(5), 708–724. https://doi.org/10.1175/JPO-D-11-0139.1